Journal of Power Sources 241 (2013) 80–86

Contents lists available at SciVerse ScienceDirect

Journal of Power Sources

journal homepage: www.elsevier.com/locate/jpowsour

Selective electrodesorption based atomic layer deposition (SEBALD) modifications of silver surfaces for enhancing oxygen reduction reaction activity

M. Innocenti [a,b,*], G. Zangari [c], C. Zafferoni [a], I. Bencistà [a], L. Becucci [a], A. Lavacchi [b], F. Di Benedetto [d], S. Bellandi [a], F. Vizza [b], M.L. Foresti [a]

[a] Department of Chemistry, University of Florence, via della Lastruccia 3, 50019 Sesto Fiorentino (FI), Italy
[b] ICCOM, CNR, via Madonna del Piano 10, 50019 Sesto Fiorentino (FI), Italy
[c] Department of Materials Science and Engineering and Center for Electrochemical Science and Engineering, University of Virginia, Charlottesville, VA 22904-4745, USA
[d] Department of Earth Sciences, University of Florence, via G. La Pira 4, 50121 Firenze, Italy

HIGHLIGHTS

- We obtain new Pt-free catalytic surfaces for the oxygen reduction reaction (ORR).
- We use metals such as Fe–Co–Ag which are suitable for alkaline fuel cells.
- We apply the SEBALD method to deposit clusters of Fe and Co on silver.
- Increasing information about three-metallic electrocatalysts.

ARTICLE INFO

Article history:
Received 26 July 2012
Received in revised form
5 April 2013
Accepted 21 April 2013
Available online 30 April 2013

Keywords:
ORR
SEBALD
Electrodeposition
Silver
catalytic surfaces

ABSTRACT

The increasing attention addressed toward the synergic effect of various metals on the catalysis of one of the most important electrocatalytic reaction, such as the Oxygen Reduction Reaction (ORR), led us to study the effect of monolayers of Fe and of mixed Fe and Co on Ag(111), whose catalytic activity is already known and well characterized. Fe and Co/Fe clusters were obtained by the Selective Electrodesorption Based Atomic Layer Deposition (SEBALD) method, which is a novel electrochemical route to deposit metal clusters on a foreign substrate recently proposed by our group. SEBALD of Fe or Co/Fe resulted in an enhanced catalytic activity; Co/Fe in particular was demonstrated to assemble in small clusters, providing access of the electrolyte to Ag and enabling a bimetallic catalytic effect.

1. Introduction

The oxygen reduction reaction (ORR) is regarded as one of the most important electrocatalytic reactions in the field of electrochemical energy conversion systems as well as in a number of industrial processes. The ORR however is a multi-electron reaction with a complex reaction pathway, which usually occurs at a significant rate only at high overpotential unless expensive catalysts, such as Pt, are used [1]. In spite of the many attempts made in the last decade to develop non-Pt based catalysts for low temperature air cathodes, Pt remains the catalyst of choice, at least for acid-based fuel cells. The situation in alkaline electrolytes is rather different; due to the stability of non-noble metals in this environment, many more opportunities are available for the development of non-Pt catalysts for the ORR. The discovery of the catalytic properties of cobalt phthalocyanine [2] for example was followed by numerous studies of organometallic complexes as promising alternatives for Pt-based electrocatalysts for ORR [3–7]. Metal chalcogenides and macrocycles were found to have high methanol tolerance, although their catalytic activity as well as their stability under operation are low [5]. The catalytic characteristics of Co- and Fe-based macrocycles improve after high-temperature treatment, but remain unsatisfactory even though they present the advantage of an extremely low cost with respect to Pt-based catalysts [6].

* Corresponding author. Department of Chemistry, University of Florence, via della Lastruccia 3, 50019 Sesto Fiorentino (FI), Italy.
E-mail address: minnocenti@unifi.it (M. Innocenti).

0378-7753/$ – see front matter © 2013 Elsevier B.V. All rights reserved.
http://dx.doi.org/10.1016/j.jpowsour.2013.04.111

The systematic investigations performed on single transition metalloporphyrins (V, Mn, Fe, Co, Ni, Cu and Zn) as well as on bimetallic transition metalloporphyrins (V/Fe, Co/Fe, Ni/Fe and Cu/Fe) [8], together with the various synthesis methods reported in the literature [6,7], led to identify Co- and Fe-based materials as those exhibiting the best activity for ORR in a wide range of metal loadings even though they need high-temperature pre-treatments [3,9–14].

The catalytic properties of silver have been extensively reported [15–21]; of particular interest is the structure sensitivity toward the ORR exhibited by different silver single crystal surfaces [22,23]. Addition of Co resulting in the formation of alloy or bimetallic surfaces enhances the catalytic properties of silver [24–26] via mechanisms that are justified on theoretical grounds [24,25,27]. Specifically, guidelines for the design of bimetallic electrocatalysts for the oxygen reduction reaction (ORR) have been proposed, assuming a simple mechanism whereby one metal is active in breaking the oxygen–oxygen bond of molecular O_2, while the other one reduces the resulting adsorbed atomic oxygen [27].

An inventory of the various methods reported in the literature to deposit catalysts on structured surfaces has been provided by Meille [28]. Some of the cited methods involve a chemical preparation process of variable complexity. Other methods rely instead on the formation of a surface coating, mainly using vapor phase deposition; only few references discuss electrodeposition, although the electrochemical methods of growth require low-cost energy since they are performed at room temperature.

An effective way to control the extent of deposited material and its morphology in electrodeposition is to use surface limited phenomena such as underpotential deposition (UPD). The interest in this technique has recently increased, essentially due to potential applications in several energy conversion technologies, including photovoltaics and electrocatalysis [29]. In photovoltaics, one example is the possibility of depositing alternate UPD layers of metals and non metals to grow binary or ternary compound semiconductors. This methodology is the basis of the Electrochemical Atomic Layer Epitaxy (ECALE) method proposed by Stickney and coworkers [30] and adopted by our group to grow cadmium and zinc chalcogenides on silver single crystals, with particular attention to binary and ternary sulfides [31–34]. In electrocatalysis, the interest is more generally directed to the selective coating of surfaces with metals able to exert catalytic effect either alone or in combination, to exploit possible synergistic effects. Unfortunately, many metals of technological interest such as Co cannot be directly deposited at underpotential on silver. However, due to the favorable energy gain involved in the formation of the corresponding sulfides, these same metals can be deposited at underpotential on sulfur covered silver. The deposition is surface limited and the successive electrodesorption of sulfur leaves behind confined clusters of metals. This method of Selective Electrodesorption Based Atomic Layer Deposition (SEBALD) has been recently proposed our group [35] and is here used to obtain Fe and Co/Fe clusters on Ag(111). The catalytic effects of these silver substrates electrochemically modified at the nanometer scale are then investigated.

2. Experimental section

Fluka analytical reagent grade Na_2S, Merck analytical reagent grade $CoSO_4 \cdot 7H_2O$, $FeSO_4 \cdot 7H_2O$, $HClO_4$, NH_4OH, were used without further purification. Merck Suprapur $HClO_4$ and NH_4OH were used to prepare the pH 9.6 ammonia buffer used as supporting electrolyte. $NaClO_4$ was used as supporting electrolyte for iron solution. The solutions were freshly prepared just before starting each series of measurements. An automated deposition apparatus consisting of Pyrex solutions reservoirs, solenoid valves, a distribution valve and a flow-cell was used under computer control. The electrolytic cell was a Teflon cylinder with a 10 mm inner diameter, delimited at the two ends by the working electrode (a Ag(111) single crystal disk of 12 mm diameter) on one side and the counter electrode on the other side. The inlet and the outlet for the solutions were placed on the side walls of the cylinder. The counter electrode was a gold foil, and the reference electrode was an Ag/AgCl (sat. KCl) placed on the outlet tubing. Both the distribution valve and the cell were designed and constructed in the workshop of our Department [31]. The solution is injected into the cell by applying a pressure as low as 0.3 atm, resulting in a flow-rate of about 1 ml s^{-1}. When the cell is filled, the pressure is no longer applied, so that the flow is stopped during ECALE deposition. A simple custom-made software allows the filling and fluxing of the cell with the various solutions. The silver single crystals were prepared according to the Bridgman technique and polished by a CrO_3 based procedure [36–38].

3. Results and discussion

3.1. Deposition of metals by SEBALD

The SEBALD method has been developed in our group to obtain well controlled atomic level deposition of a metal *M* on a foreign substrate when direct UPD is not possible [35]. A monolayer of a metal, *M*, can be deposited on a foreign substrate only when *M* is able to form a compound, M_xA_y, with an anion, *A*, that can be later eliminated by applying a potential sufficiently negative. On Ag(111) the method exploits the possibility of depositing metal sulfides by ECALE, and then applying a potential sufficiently negative, −1.6 V in order to reduce S to S(−II) which is eliminated by washing the cell with the supporting electrolyte. Usually, the growth of a metal sulfide by ECALE starts with the deposition of a UPD layer of S which drives the subsequent underpotential deposition of the metal. The growth of the S_{UPD} layer occurs by oxidative underpotential deposition of S(−II) solutions at $E = -0.68$ V. This potential just precedes the onset potential of bulk deposition, that occurs at more positive potentials. It must be noted that some metals, like Co, cannot be deposited at underpotential on Ag(111), but due to the free energy change involved in the sulfide formation, they can instead be deposited at underpotential on a S layer.

3.2. Cyclic voltammetry of Fe on Ag(111) and on S covered Ag(111)

Cyclic voltammograms of 1 mM $FeSO_4$ dissolved in 0.1 M $NaClO_4$ on Ag(111) show two marked cathodic peaks C1 and C2 (solid curve in Fig. 1).

The electrochemical behavior of iron involves the formation of surface adsorbed intermediate species. Due to the classical interest in iron as an electrode for batteries or in corrosion prevention, most of the literature data refer to the iron dissolution [39–41]. However, the mechanism of iron electrodeposition as elucidated by the combined electrochemical and mass investigation by microbalance [42] is based on the same surface adsorbed intermediates of Refs. [39–41]. It must be noted that the spread presence of chemisorbed species suggests a strong dependence on the metal used as electrode. However, with some adjustments due to the different metals, as well as to the different iron salts and electrolyte used, we retained most of the results of the literature. Thus, peak C1 can be associated to the formation of adsorbed intermediate species containing Fe(I) that are generally indicated as $Fe(OH)_{ads}$.

$$Fe^{2+} + H_2O + e \rightarrow Fe(OH)_{ads} + H^+ \quad (1)$$

According to the literature, the physical meaning of $(FeOH)_{ads}$ is ambiguous, since it may be either chemisorbed Fe(I) associated

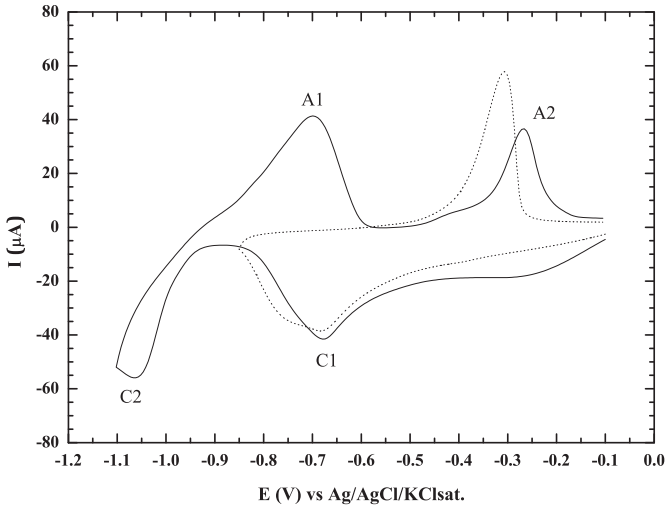

Fig. 1. Cyclic voltammogram of 1 mM $FeSO_4$ dissolved in 0.1 M $NaClO_4$on Ag(111), as recorded from −0.1 to −1.1 V (solid curve) or −0.1 to −0.85 V (dashed curve). Scan rate 50 mV s^{-1}.

with OH^- or chemisorbed $(OH)_{ads}$ [43,44]. However, we note that peak C1 could be also be associated to the underpotential deposition of Fe with partial charge transfer that leads to the formation of the above chemisorbed species that are then reduced to Fe(0) at more negative potentials giving peak C2:

$$Fe(OH)_{ads} + e \rightarrow Fe(0) + OH^- \quad (2)$$

After potential reversal, the deposited Fe(0) starts to undergo the first oxidation, i.e. the reverse of reaction (2), followed by a second electron release. Still according to Ref. [42], both oxidation of Fe(0) and Fe(I) species proceed on the surface electrode, since no significant mass variation was remarked. Therefore, by extending these results to our case, the anodic peak A1, can be associated both to the reverse of reaction (2) and to the formation of an adsorbed species of Fe(II):

$$Fe(OH)_{ads} + H_2O \rightarrow Fe(OH)_{2,ads} + H^+ + e \quad (3)$$

Finally, peak A2 can be associated to further oxidation of the remaining Fe(I) which results in soluble Fe(II) compounds or also to the formation of iron(III) soluble species [42]. Dotted curve in Fig. 1 shows that when the potential is reversed at a less negative value the anodic peak A2 increases, probably since the Fe(I) species formed at C1 had not been consumed by further reduction/oxidation reactions (peaks C1 and A1).

As any other metal studied in our group, Fe is deposited on S-covered Ag(111) at less negative potentials than on Ag(111) due to the energy gain involved in the sulfide compound formation [31–35]. As reported in the literature, iron and sulfur form a large variety of metallic and semiconducting compounds, many of which being non-stoichiometric or interstitials; thus, in addition to FeS, Fe(II) sulfides also include $Fe_{1-x}S$ and FeS_{1-x} [45]. As a matter of fact, the cyclic voltammogram of Fe(II) on a S-covered Ag(111) suggests the possibility to form different compounds, since this CV shows significant differences depending on whether S was deposited at underpotential ($E = -0.68$ V) or at overpotential ($E = -0.6$ V for 30 s), forming a bulk-like film (Fig. 2a). Specifically, iron deposition on S_{upd} gives rise to a broad bump followed by a more negative peak, whereas on S_{bulk} a more regular peak shape is observed. Note that the potential scan of Fig. 2a is limited to the negative value of −0.75 V to avoid reduction of the sulfur layer. Nonetheless, the cathodic processes involved in both cases seem to

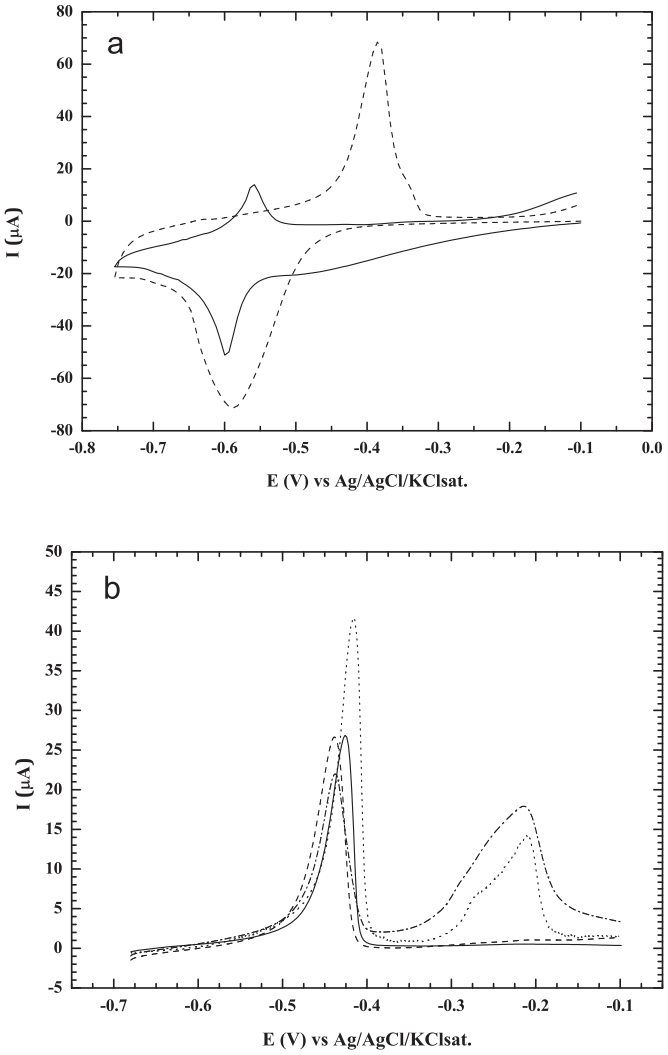

Fig. 2. (a) Cyclic voltammograms of 1 mM $FeSO_4$ dissolved in 0.1 M $NaClO_4$ on Ag(111) modified with a layer of S_{upd} (solid curve) or S_{bulk} (dashed curve) as recorded from −0.1 to −0.75 V. Scan rate 50 mV s^{-1}. (b) Linear sweep voltammograms for the oxidative stripping of Fe deposited at −0.45V on S_{upd} (solid curve) or S_{bulk} (dashed curve) and at −0.65V on S_{upd} (dotted curve) or S_{bulk} (dash dotted curve). Scan rate 10 mV s^{-1}.

be surface limited, maintaining the character of underpotential deposition processes. In fact, the anodic stripping curves of iron deposited at −0.65 V for different deposition times yield comparable charge values (Fig. 2b).

It must be stressed that the system at hand is exceptionally complex due to the different species that can be formed by iron with sulfur and oxygen, and, therefore a certain degree of irreproducibility is unavoidable. However, all the considerations reported here are based on self-consistent data, that is on data collected in nominally identical experiments (same silver surface, same solutions, and same experimental conditions). That means that the numerical values extracted in the various experiments can also be somewhat different, but, together, they concur to outline a picture of the general behavior of this system. In this light, the substantial agreement between the charge values obtained from the stripping curves of Fe deposited at the same potential on S_{upd} and S_{bulk} suggest that the extent of Fe deposition only depends on potential. Therefore it can be assumed that the charge involved in Fe deposition at −0.45 V is 160–170 μC cm^{-2}, whereas that at −0.65 V is 360–380 μC cm^{-2}. In the latter case the stripping process yields two successive peaks as if compounds of different

stability were involved. Qualitatively, one could speculate about the presence of sulfides with different composition containing the same amount of Fe (same global dissolution charge) but different amount of S, that could be dissolved at different potentials: sulfides with higher S content could be expected to have a higher heat of formation and, hence, a more positive dissolution potential. The above hypothesis could also be supported by the observation that the more positive anodic peak is greater on S_{bulk} than on S_{upd}, as if in the former case more S could bind to Fe. This is supported by the fact that the UPD layer of S has a very strained structure with S–S distances as high as 7.6 Å [32] that determines a coverage $\theta = 0.43$.

A further experimental observation is that the stripping voltammograms of Fe deposited at −0.65 V on S_{bulk} deposits obtained with increasing deposition times (10, 20, 30 s, not shown) show the same shape and the same charge. This suggests that only the upper layer of S was involved in compound formation. In conclusion, the good reproducibility among the various curves obtained on S_{bulk} indicates that the S amount is not critical, and the slight difference in the shape of the curve obtained on S_{upd} does not seem to be connected to a different amount of deposited Fe.

Repeating the basic ECALE cycles results in the overall mass of Fe and S deposits increasing proportionally, even if both are lower than those deposited in the first cycle; this is a general observation for all compounds grown by ECALE. No additional charge is measured beyond the second cycle, as if the interfacial UPD phenomena on which ECALE methodology is based didn't occur anymore; this problem however is beyond the purpose of this paper which is focused on the formation of Fe and Co/Fe clusters on Ag(111).

3.3. Deposition of Co, Fe and Co/Fe clusters by SEBALD

The deposition of Co or Fe alone by SEBALD has been already described in Ref. [35]. Here, we applied a similar procedure to carry out the mixed deposition of both metals. More precisely, we first applied the ECALE method to grow the ternary Co/Fe sulfide, from which S was successively eliminated by cathodic electrodesorption.

The experimental steps were as follows:

- Underpotential deposition of S from a solution of 0.5 mM Na_2S in ammonia buffer at $E = -0.68$ V for 60 s
- Rinsing with ammonia buffer at $E = -0.68$ V
- Underpotential deposition of Co from a solution of 0.5 mM $CoSO_4$ in ammonia buffer at $E = -0.68$ V for 60 s
- Rinsing with ammonia buffer at $E = -0.68$ V
- Underpotential deposition of S as above
- Rinsing with ammonia buffer at $E = -0.68$ V
- Rinsing with 0.1 M $NaClO_4$ at $E = -0.65$ V
- Underpotential deposition of Fe from a solution of 1 mM in 0.1 M $NaClO_4$ at $E = -0.65$ V for 60 s
- Rinsing with 0.1 M $NaClO_4$ at $E = -0.65$ V
- Rinsing with ammonia buffer at $E = -0.68$ V
- Underpotential deposition of S as above
- Rinsing with ammonia buffer at $E = -0.68$ V
- Electrodesorption of S by applying a potential $E = -1.6$ V for 60 s

Fig. 3a shows the stripping curve of the Co/Fe deposit thus obtained, together with the stripping curves of Fe and Co deposited separately. All stripping curves were recorded in ammonia buffer solutions to favor the metal dissolution through the formation of Co or Fe ammonia complexes.

As expected, the charge associated to the Co/Fe deposit is larger than that of the separate deposits, since two ECALE cycles have been employed instead of one. However, the stripping charge of the

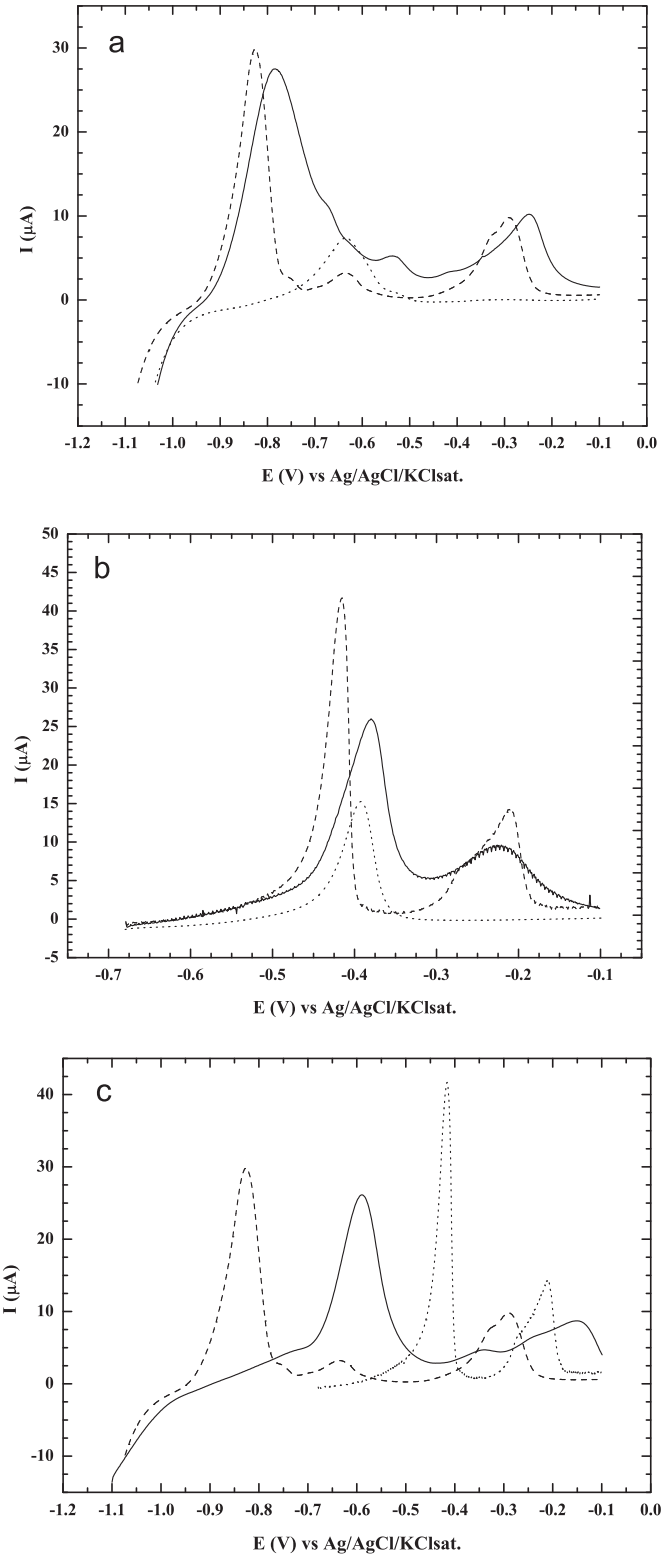

Fig. 3. (a) Linear sweep voltammograms for the oxidative stripping of Fe (dashed curve), Co/Fe (solid curve) and Co (dotted curve) deposited on S-covered Ag(111) after cathodic removal of S. (b) Linear sweep voltammograms for the oxidative stripping of Fe (dashed curve), Co/Fe (solid curve) and Co (dotted curve) deposited on S-covered Ag(111) before cathodic removal of S. (c) Linear sweep voltammograms for the oxidative stripping of Fe deposited on S-covered Ag(111) after (dashed curve) or before (dotted curve) removal of S. The solid curve is the oxidative stripping of Fe deposited in bulk at −0.95 V for 60 s directly on Ag(111). The supporting electrolyte was ammonia buffer and the scan rate was 10 mV s^{-1}.

deposits containing Fe either alone or in the mixture exhibit a certain degree of irreproducibility that could be ascribed either to the phenomenon of hydrogen absorption during the cathodic electrodesorption of S, to the formation of various Fe–S compounds or to the formation of iron–silver alloys, or to both. The result is the presence in the stripping curves of several bumps and peaks whose assignment is beyond the purpose of this paper, but nonetheless renders difficult the measure of the charge involved. On the contrary, the stripping curve for Co is highly reproducible and yields a charge, about 125 μC cm^{-2}, which is in good agreement with that reported in Ref. [35]. On the other hand, the stripping curves of deposits of Co, Fe and Co/Fe carried out without S elimination present a good reproducibility and allow to reasonably assign a charge of 130 μC cm^{-2} to Co, 360 μC cm^{-2} to Fe and 425 μC cm^{-2} to Co/Fe (Fig. 3b).

It should be stressed additionally that the charge involved in the formation of the bimetallic Co/Fe deposit is not exactly the sum of the Fe and Co separate deposits, since as always observed, in the second ECALE cycle the extent of metal deposition is lower than in the first one.

Finally, Fig. 3c shows that the solid curve obtained by stripping a Fe film directly deposited on Ag(111) applying a potential of −0.95 V for 60 s lies in between the curves obtained depositing Fe on a S-covered Ag(111) and then anodically dissolving it after having removed S (Fig. 2a, dashed curve), or before (dotted curve). As expected due to the higher bonding energy of the sulfide compounds, the stripping of Fe from its sulfide takes place at the most positive potential. No difference on the other hand would expected between the other two curves, since removal of S in the former case should also result in a deposit of Fe on Ag(111). The observed shift of the stripping potential suggests however that the dissolving iron species in the two experiments are different. Tentatively, it could be hypothesized that in the presence of a S layer, formation of iron sulfides may prevail over that of the $Fe(OH)_{ads}$ species probably formed by direct electrodeposition on Ag, leading to a stronger bonding. Alternatively, the prolonged application of the negative potential necessary to eliminate S may have also the effect of reducing the iron film, removing oxygen adsorbed species. These hypotheses could both explain the more negative stripping potentials observed for Fe on Ag films.

3.4. Electrocatalytic effect

The catalytic properties of the deposits of Fe and Co/Fe were evaluated by oxygen reduction measurements. ORR voltammetric curves on Ag(111) and on Ag(111) modified by SEBALD deposition of Fe or Co/Fe were recorded in O_2 saturated 0.1 M KOH electrolyte, at a rotating disk electrode using different rotation rates and with a scan rate of 50 mV s^{-1}. The potential was linearly swept from −1.1 V to −0.1 V and then reversed. No significant hysteresis between the polarization curves recorded in the positive and negative going sweep directions was found, nor between the different silver single crystal surfaces [22]. Fig. 4 shows the polarization curves for the ORR on Ag(111) and on Ag(111) covered by Fe and Co/Fe (positive sweep direction at 500 rpm) as recorded on a rotating-disk working electrode of 0.785 cm^2 at the angular rotation rate $\omega = 500$ rpm.

Albeit small, the progressive shift toward less negative potential of the ORR curves in Fig. 4 shows that the catalytic effect of Ag is enhanced by the presence of Fe and that it is further increased at the bimetallic Co/Fe deposit. It must be noted that we are not studying the catalytic effect of the Co/Fe deposit itself, but the synergic effect exerted by this deposit on silver, which is already considered a good catalyst. In this perspective, the estimation of the Co/Fe loading has a limited importance. Nevertheless, this value can

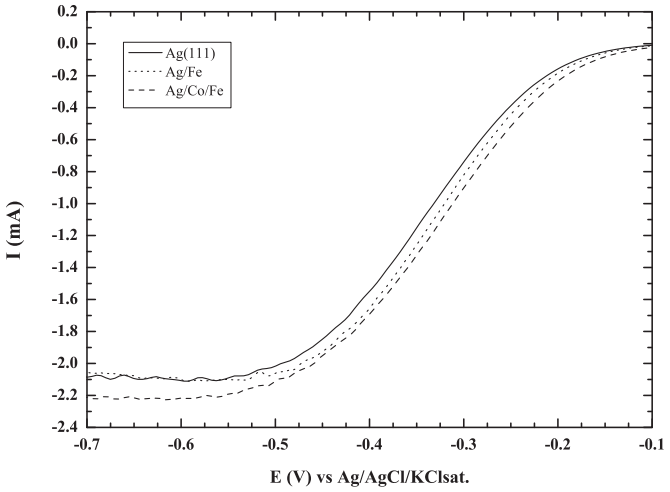

Fig. 4. Current–potential curves for Oxygen Reduction Reaction in KOH 0.1 M at a rotating disk electrode (500 rpm) for bare Ag(111) alone (solid curve) and on Ag(111) covered by Fe (dotted curve) or Co/Fe clusters (dashed curve). Scan rate 50 mV s^{-1}.

be obtained using the Faraday's laws considering that the reduction of both Co and Fe involves two electrons per mole. Thus, the charge of the Co/Fe film, 425 μC cm^{-2}, corresponds to 2.2×10^{-9} mol cm^{-2} of (Co + Fe) that, assuming a 1:1 Co/Fe ratio, yields a mass of 125 ng cm^{-2}. The exiguity of this value is clearly justified by the nanometric size of the deposit.

The number of electrons transferred per O_2 molecule in the ORR on the different catalysts can be estimated by Levich plots according to Eq (4):

$$i_d = 0.620nFAD_0^{2/3}\omega^{1/2}\nu^{-1/6}C_0 \quad (4)$$

Here, i_d is the current density, n is the number of exchanged electrons, F is the Faraday constant, A is the area of the electrode (0.785 cm^2), D_0 is the oxygen diffusion coefficient (1.95×10^{-5} cm^2 s^{-1}), ω is the angular rotation rate of the electrode (in rad s^{-1}), ν is the kinematic viscosity of the solution

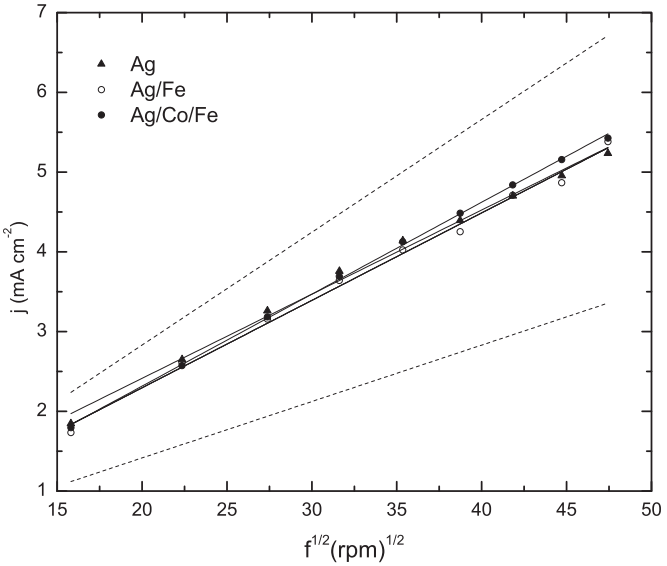

Fig. 5. Levich plots for ORR on bare Ag(111) (▲), and Ag(111) covered by Fe (○) or Co/Fe clusters (●). Dashed lines correspond to the theoretical slope calculated for 2 and 4 electrons processes.

Table 1
The potential at $j = -1$ mA cm^{-2} and average number of electron exchanged during the oxygen reduction for the various catalysts.

Sample	$E_{I=1\ mA}$	n
Ag	−0.33	3.0
Ag/Fe	−0.32	3.1
Ag/Co/Fe	−0.31	3.3

(0.008977 cm^2 s^{-1}) and C_0 is the O_2 solubility in solution (1.15×10^{-3} mol dm^{-3}) [46].

Interestingly, the number of exchanged electrons, calculated by the slopes of the plots, increases toward the ideal value of 4e$^-$ with the same ranking found for the catalytic activity. It must be noted that the sample containing Co/Fe, besides having the best catalytic activity, is also the one that follows a pathway with the number of electrons closest to the optimal number of 4 (Fig. 5).

Table 1 summarizes the important parameter of the various catalysts, i.e. the potential at which the ORR current density is equal to −1 mA cm^{-2} and the number of exchanged electrons.

3.5. Atomic force microscopy (AFM) analysis

In order to achieve a better insight on the morphological features of bimetallic Co/Fe films, an ex-situ AFM analysis was performed. During AFM imaging in contact mode it is possible to record both the vertical deflection of cantilever, which generates the topographic image, and its lateral deflection. Collecting the images of the cantilever lateral deflection, usually called Lateral Force Microscopy (LFM), allows to distinguish areas showing different friction between the scanning tip and the sample and to obtain thus edge-enhanced images of any surface.

Fig. 6 reports both the topography (a) and the LFM images [left-scanned (b) and right-scanned (c)]. The topographic image shows the formation of clusters with an average size of 30 nm. The extremely low roughness of this image (R_{RMS} = 1.5 nm) allows to evidence the formation of triangular shapes on the surface, which are the characteristic geometric features of the (111) crystallographic plane. The LFM images show the presence of areas (dark in the left scan and bright in the right scan) which are of a different nature with respect to the homogeneous background, thus suggesting that they can be identified as Co/Fe clusters.

For an approximate evaluation of surface coverage of the particles of iron and cobalt were analyzed 16 different areas of the sample and calculated the average coverage of a total of 48 images. The result obtained by summing the areas occupied by the clusters thus identified yields a Co/Fe coverage equal to 23%.

4. Conclusion

The increasing attention addressed toward the synergistic effect of various metals on the catalysis of one of the most important electrocatalytic reaction, such as the Oxygen Reduction Reaction (ORR), led us to study the effect of monolayers of Fe and of mixed Fe and Co on Ag(111), whose catalytic activity is already well known and extensively characterized.

Metal clusters of interest for catalytic applications can be simply deposited on a foreign substrate by the Selective Electrodesorption Based Atomic Layer Deposition (SEBALD) method recently proposed by our group. By this method, a metal can be deposited at underpotential on a previously deposited sulfur layer, which is successively eliminated leaving a controlled amount of elemental metal clusters on the substrate.

Incidentally, the formation of a single layer of Co and Fe sulfides could represent a great model system to study their electrochemical formation. The presented system could have a broader significance for corrosion studies where the characterization of this S-compound could be studied as a function of the potential of their formation.

The experimental conditions for deposition of Fe and Co/Fe were investigated both on the silver substrate and on the silver modified with a S layer, deposited either at underpotential or in bulk. In spite of the limited reproducibility induced by the complex interaction of Fe with sulfur with respect to the deposition of Co alone, it was possible to obtain reliable qualitative as well as semi-quantitative results. Thus, when compared with the charge, 221 μC cm^{-2}, associated to a monolayer of Ag on Ag(111), the amount of 130 μC cm^{-2} for Co, 360 μC cm^{-2} for Fe and 425 μC cm^{-2} for Co/Fe measured assuming the transfer of two electrons per atom from Fig. 3b yield coverage values of 0.29, 0.82 and 0.97 respectively, that would correspond to a nearly complete coverage for both the samples Fe and Co/Fe, which could significantly mask and partially hinder the catalytic effect of silver. On the contrary, the AFM images of the Co/Fe sample suggest that the deposit rearranges forming clusters and leaving a significant amount of silver at the surface, in contact with the electrolyte. Therefore, the observed enhancement of the catalytic properties is an experimental confirmation of a synergy between silver and Co/Fe clusters ascribable to electronic factors. A previous work on the catalytic effect of monolayer islands of Co grown on Ag(111) using a template-assisted procedure [26] evidenced the strong effect of morphology on the catalytic effect. Here, the attention was mainly directed to elucidate the behavior of Fe and Co/Fe clusters grown on Ag(111) by the SEBALD method. As reported in Table 1, the potential shift in correspondence of $j = 1$ mA cm^{-2} is small but allows to clearly determine the following trend in catalytic activity: Ag(111) < Fe–Ag(111) < Co/Fe–Ag(111).

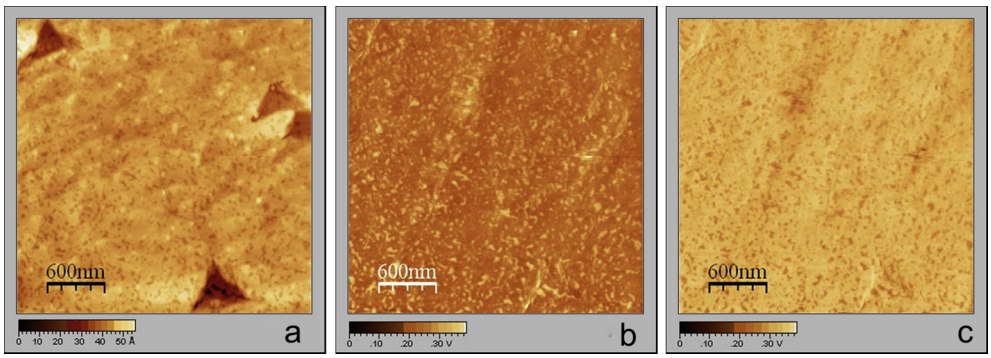

Fig. 6. AFM images of SEBALD Co/Fe film on Ag(111): (a) 3 × 3 μm^2 AFM topographic image, (b) left-scanned LFM image, and (c) right-scanned LFM image.

Interestingly, the number of exchanged electrons, calculated by the slopes of the Levich plots, increases toward the best value of $4e^-$ with the same order found for the catalytic activity.

The described system is not directly usable as electrode in practical applications and its main intent is to study the possibility of using the SEBALD method to deposit a monolayer of metals able to enhance the catalytic effect of silver on ORR. However, the presented results represent a model system, whose evolution will be that of also limiting the amount of silver by depositing a controlled amount of silver on materials, such as glassy carbon, that are usable for fuel cells and further deposit on it Fe and Co/Fe clusters by SEBALD.

(b) Linear sweep voltammograms for the oxidative stripping of Fe deposited at −0.45 V on S_{upd} (solid curve) or S_{bulk} (dashed curve) and at −0.65 V on S_{upd} (dotted curve) or S_{bulk} (dash dotted curve). Scan rate 10 mV s^{-1}.

Acknowledgments

The authors are grateful to Ferdinando Capolupo for his technical assistance. It is acknowledged the financial support from the MIUR (Italy) for the PRIN 2008 project *prot. 2008N7CYL5*.

References

[1] N.M. Markovic, T.J. Schmidt, V. Stamenkovic, P.N. Ross, Fuel Cells 1 (2001) 105–116.
[2] R. Jasinski, Nature 201 (1964) 1212.
[3] C.W.B. Bezerra, L. Zhang, K. Lee, H. Liu, A.L.B. Marques, E.P. Marques, H. Wang, J. Zhang, Electrochim. Acta 53 (2008) 4937–4951.
[4] C.W.B. Bezerra, L. Zhang, K. Lee, H. Liu, J. Zhang, Z. Shi, A.L.B. Marques, E.P. Marques, S. Wu, J. Zhang, Electrochim. Acta 53 (2008) 7703–7710.
[5] B. Wang, J. Power Sources 152 (2005) 1–15.
[6] Y. Feng, N. Alonso-Vante, Phys. Status Solidi B 245 (2008) 1792–1806.
[7] Valentina Bambagioni, Claudio Bianchini, Jonathan Filippi, Alessandro Lavacchi, Werner Oberhauser, Andrea Marchionni, Simonetta Moneti, Francesco Vizza, Rinaldo Psaro, Vladimiro Dal Santo, Alessandro Gallo, Sandro Recchia, Laura Sordelli, J. Power Sources 196 (2011) 2519–2529.
[8] Deryn Chu, Rongzhong Jiang, Solid State Ionics 148 (2002) 591–599.
[9] Shang Li, Lei Zhang, Jenny Kima, Mu Pan, Zheng Shi, Jiujun Zhang, Electrochim. Acta 55 (2010) 7346–7353.
[10] A. Widelov, Electrochim. Acta 38 (1993) 2493.
[11] G. Lalande, G. Faubert, R. Cote, D. Guay, J.P. Dodelet, L.T. Weng, P. Bertrand, G. Dénès, Electrochim. Acta 41 (1996) 1689–1701.
[12] F. Jaouen, M. Lefevre, J.P. Dodelet, M. Cai, J. Phys. Chem. B 110 (2006) 5553.
[13] C.W.B. Bezerra, L. Zhang, H. Liu, K. Lee, A.L.B. Marques, E.P. Marques, H. Wang, J. Zhang, J. Power Sources 173 (2007) 891.
[14] G. Faubert, R. Côté, J.P. Dodelet, M. Lefèvre, P. Bertrand, Electrochim. Acta 44 (1999) 2589.
[15] C. Coutenceau, L. Demarconnay, C. Lamy, J.-M. Léger, J. Power Sources 156 (2006) 14.
[16] A. Zwetanova, K. Juttner, J. Electroanal. Chem. 119 (1981) 149–164.
[17] J.D.E. McIntyre, W.F. Peck, Electrochemistry at Single-Crystal Metal Electrodes. Electrocatalytic Effects on Surface Atomic Structure, Defects and Adatoms on Oxygen Reduction, The Electrochemical Society, Pennington, NJ, 1984, pp. 102–130.
[18] R.R. Adzic, Electrocatalysis, Wiley-VCH, New York, 1998, pp. 197–242.
[19] T. Hurlen, Y.L. Sandler, E.A. Pantier, Electrochim. Acta 11 (1966) 1463–1473.
[20] Israel E. Wachs, Robert J. Madix, Surf. Sci. 76 (1978) 531–558.
[21] J.S. Spendelow, A. Wieckowski, Phys. Chem. Chem. Phys. 9 (2007) 2654.
[22] B.B. Blizanac, P.N. Ross, N.M. Markovic, J. Phys. Chem. B 110 (2006) 4735–4741.
[23] N.M. Markovic, P.N. Ross, Surf. Sci. Rep. 45 (2002) 117–229.
[24] J.L. Fernandez, D.A. Walsh, A.J. Bard, J. Am. Chem. Soc. 127 (2005) 357–365.
[25] F.H.B. Lima, J.F.R. de Castro, Edson A. Ticianelli, J. Power Sources 161 (2006) 806–812.
[26] F. Loglio, E. Lastraioli, C. Bianchini, C. Fontanesi, M. Innocenti, A. Lavacchi, F. Vizza, M.L. Foresti, ChemSusChem 4 (8) (2011) 1112–1117.
[27] Y. Wang, P.B. Balbuena, J. Phys. Chem. B 109 (2005) 18902–18906.
[28] V. Meille, Appl. Catal A: Gen. 315 (2006) 1–17.
[29] G. Zangari, ECS Interface Summer 2011 20 (2011) 31–32.
[30] B.W. Gregory, J.L. Stickney, J. Electronanal. Chem. 300 (1991) 543.
[31] M. Innocenti, G. Pezzatini, F. Forni, M.L. Foresti, J. Electrochem. Soc. 148 (5) (2001) C357–C362.
[32] M. Innocenti, S. Cattarin, M. Cavallini, F. Loglio, M.L. Foresti, J. Electroanal. Chem. 532 (2002) 219–225.
[33] F. Loglio, M. Innocenti, G. Pezzatini, M.L. Foresti, J. Electroanal. Chem. 562 (2004) 117–125.
[34] M. Innocenti, S. Cattarin, F. Loglio, T. Cecconi, G. Seravalli, M.L. Foresti, Electrochim. Acta 49 (2004) 1327–1337.
[35] M. Innocenti, S. Bellandi, E. Lastraioli, F. Loglio, M.L. Foresti, Langmuir 27 (18) (2011) 11704–11709.
[36] A. Hamelin, in: B.E. Conway, R.E. White, J.O.'M. Bockris (Eds.), Modern Aspects of Electrochemistry, Vol. 16, Plenum Press, New York, 1985, p. 1.
[37] T. Kurasawa, Patent Japan 35:5619, 1960.
[38] M.L. Foresti, F. Capolupo, M. Innocenti, F. Loglio, Crystal Growth and Design 2 (2002) 73–77.
[39] W.J. Lorenz, K.E. Heusler, in: F. Mansfield (Ed.), Corrosion Mechanism: Anodic Dissolution of Iron Group Metals, Marcel Dekker, New York, 1987, pp. 1–83.
[40] D.M. Dražić, in: J.O.'M. Bockris, B.E. Conway (Eds.), Modern Aspects of Electrochemistry: The Electrochemistry of Iron in an Active State, Vol. 19, Plenum Press, New York, 1989, pp. 69–192.
[41] J.O.'M. Bockris, S.U.M. Khan, Surface Electrochemistry: A Molecular Level Approach, Plenum Press, New York, 1993, p. 765.
[42] E. Bura-Nakic, A. Róka, I. Ciglenecki, G. Inzelt, Electroanalysis 21 (15) (2009) 1699–1708.
[43] K.E. Heusler, in: A.J. Bard (Ed.), Encyclopedia of Electrochemistry of the Elements, Vol. 9A, M. Dekker Inc., New York, 1982, p. 230.
[44] I. Flis-Kabulska, J. Flis, T. Zakroczymski, Electrochim. Acta 52 (2007) 7158–7165.
[45] A. Gomes, M.H. Mendonca, M.I. Da Silva Pereira, F.M.A. Costa, J. Solid State Electrochem. 4 (2000) 168–176.
[46] Y. Wang, D. Zhang, H. Liu, J. Power Sources 195 (2010) 3135–3139.